

Luminescent Gold Surfaces for Sensing and Imaging: Patterning of Transition Metal Probes

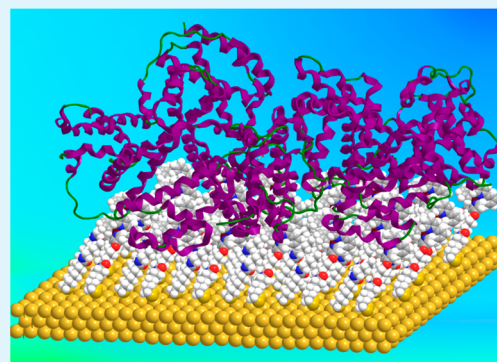
Samuel J. Adams, David J. Lewis, Jon A. Preece, and Zoe Pikramenou*

School of Chemistry, University of Birmingham, Edgbaston, Birmingham, West Midlands B15 2TT, United Kingdom

 Supporting Information

ABSTRACT: Luminescent transition metal complexes are introduced for the microcontact printing of optoelectronic devices. Novel ruthenium(II), RubpySS, osmium(II), Os bpySS, and cyclometalated iridium(III), IrbpySS, bipyridyl complexes with long spacers between the surface-active groups and the metal were developed to reduce the distance-dependent, nonradiative quenching pathways by the gold surface. Indeed, surface-immobilized RubpySS and IrbpySS display strong red and green luminescence, respectively, on planar gold surfaces with luminescence lifetimes of 210 ns (RubpySS-Au) and 130 and 12 ns (83%, 17%) (IrbpySS-Au). The modified surfaces show enhancement of their luminescence lifetime in comparison with solutions of the respective metal complexes, supporting the strong luminescence signal observed and introducing them as ideal inorganic probes for imaging applications. Through the technique of microcontact printing, complexes were assembled in patterns defined by the stamp. Images of the red and green patterns rendered by the RubpySS-Au and IrbpySS-Au monolayers were revealed by luminescence microscopy studies. The potential of the luminescent surfaces to respond to biomolecular recognition events is demonstrated by addition of the dominant blood-pool protein, bovine serum albumin (BSA). Upon treatment of the surface with a BSA solution, the RubpySS-Au and IrbpySS-Au monolayers display a large luminescence signal increase, which can be quantified by time-resolved measurements. The interaction of BSA was also demonstrated by surface plasmon resonance (SPR) studies of the surfaces and in solution by circular dichroism spectroscopy (CD). Overall, the assembly of arrays of designed coordination complexes using a simple and direct μ -contact printing method is demonstrated in this study and represents a general route toward the manufacture of micropatterned optoelectronic devices designed for sensing applications.

KEYWORDS: *imaging, optical active surfaces, printing, luminescence, recognition*



INTRODUCTION

“Bottom-up” approaches for surface fabrication toward nanoscale devices have flourished in recent years, as “top-down” methods have begun to reach the limits of their potential.^{1–5} In particular, microcontact printing (μ CP), initially developed by Whitesides,^{6,7} allows controlled deposition of molecules on planar substrates such as gold or glass for the fabrication of surfaces for sensing devices for the detection of analytes.^{8–11} Photoactive transition metal complexes offer many attractive properties for imaging applications^{12–15} including photostability and excitation and emission profiles within the visible region that are more compatible with conventional imaging techniques and larger Stokes shifts (greater than 100 nm). Luminescent thin films have been developed using noncovalent assembly of photoactive metals via Langmuir–Blodgett methods^{16,17} or “layer-by-layer” approaches.^{18,19} However, applications of gold surfaces modified with transition metal complexes have been dominated by electrochemical studies^{20–22} due to the reported luminescence quenching of the excited state by the gold.^{23–25} Despite this, the covalent attachment of metal complexes to gold is attractive as a platform to build recognition sites and develop sensing motifs.

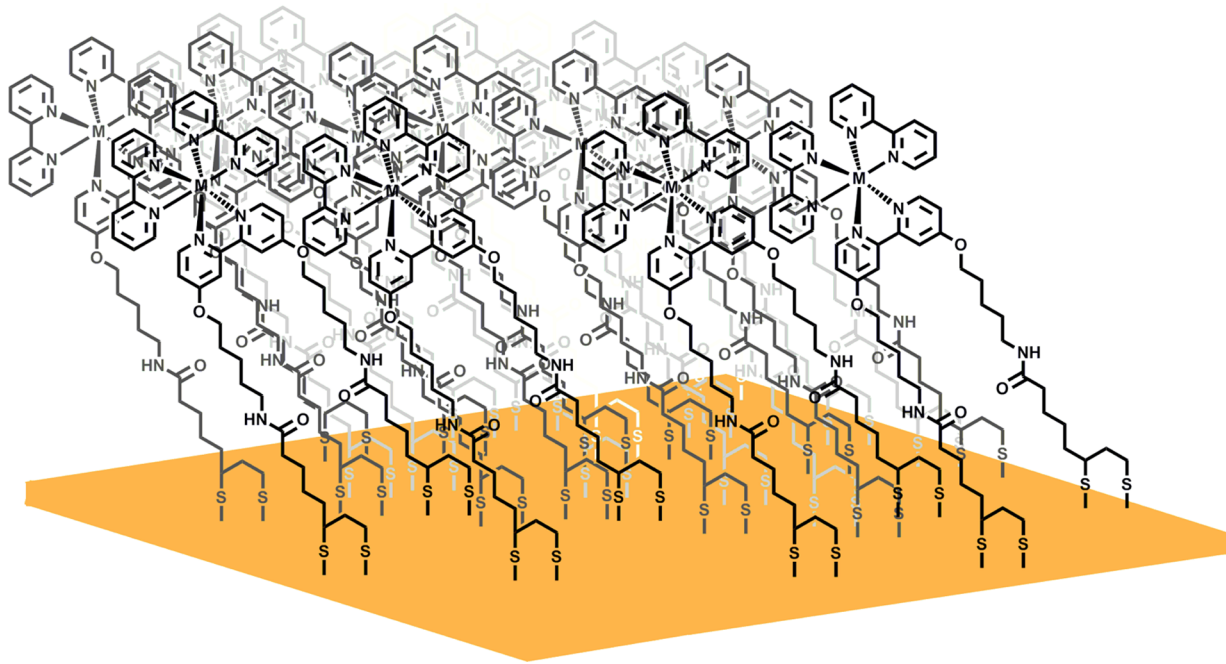
Complexes of ruthenium(II) and in particular iridium(III) have been shown to have significant affinities for biomolecules.^{26–29}

Albumins especially are popular proteins for employment in immunodiagnoses and devices.^{28,30–33} In this paper, we introduce the design of transition metal complexes for stable luminescent films patterned by μ CP, suitable for imaging of the surface pattern and also as surface-immobilized probes for protein binding. In order to produce robust monolayers for use with μ -contact printing techniques, we have designed a lipoic acid based surface attachment on a bipyridine ligand, bpySS (Scheme 1), with a long spacer chain to reduce luminescence quenching from the gold surface. We have examined the formation of monolayers of ruthenium(II), RubpySS, and cyclometalated iridium(III), IrbpySS, bipyridyl complexes on gold and analyzed their photophysical properties for promising optoelectronic device development (Scheme 1). The osmium(II), Os bpySS, monolayers on gold did not show any luminescence and were not further examined. Transition metal complexes have not been used in microcontact printing, and our method for attachment to the surface was used to test the potential formation of stable stamps that can be used in sensing applications. The patterning of

Received: April 17, 2014

Accepted: June 16, 2014

Published: June 16, 2014

Scheme 1. Transition Metal Complexes for Surface Patterning

the complexes to surfaces is examined, and luminescence microscopy studies are used to reveal the pattern. The response of the luminescent surfaces to the serum protein bovine serum albumin (BSA) has also been studied.

EXPERIMENTAL SECTION

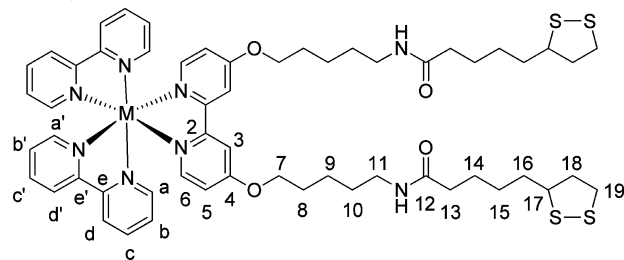
Materials and Methods. Starting materials were obtained from Sigma-Aldrich, Fluka, Fisher Scientific, or Acros Chemicals and used without any further purification. Dimethylformamide (DMF) was obtained from AGTC Bioproducts Ltd. and dried with 3 or 4 Å molecular sieves before use. Gold slides (30 nm on silicon with 5 nm Ti priming layer) were purchased from Georg Albert PVD, Germany. A Sylgard 184 Elastomer Kit (Dow-Corning) was used to create the polydimethylsiloxane (PDMS) stamps. Flash column chromatography was performed using LC60A 40–63 µm silica gel. All reactions were performed under a nitrogen atmosphere unless stated otherwise. Os(bpy)₂Cl₂ was prepared via the method of Kober et al.³⁴ (0.69 g, 53%). [Ir(ppy)₂Cl]₂ was prepared via a method outlined by Sprouse et al.³⁵ (0.36 g, 51%). 4,4'-Dihydroxy-2,2'-bipyridine (4) was prepared by the method of Gorman et al.³⁶

Instrumentation. ¹H NMR spectroscopy was carried out on a Bruker AVIII300 spectrometer. ¹³C and 2D NMR spectroscopy was carried out on a Bruker AVIII400 spectrometer. Electrospray mass spectrometry was carried out on a Micromass LC-TOF. MALDI mass spectrometry was carried out on a Micromass MX MALDI-TOF. UV-vis spectroscopy was carried out on a Varian Cary 50 or Cary 5000 spectrophotometer. UV-vis spectra were collected using 1 cm path length quartz cuvettes. Luminescence spectroscopy was carried out by a Photon Technology International luminescence spectrometer with a 75 W xenon arc lamp as the illumination source and also on an Edinburgh Instruments FLS920 steady state and time-resolved spectrometer fitted with an Olympus IX71 inverted microscope. The detection system used incorporated R928 (visible) and R5509-72 (NIR) Hamamatsu photomultiplier tubes. The emission monochromator is fitted with two interchangeable gratings blazed at 500 and 1200 nm. F900 spectrometer analysis software was used to record the data. Luminescence lifetime experiments were carried out using an Edinburgh Instruments EPL-445 or EPL-375 laser as the excitation source. Lifetimes were fitted using Edinburgh Instruments F900 software, with errors of ±10%. Luminescence experiments were carried out using 1 cm path length quartz cuvettes with four transparent polished faces. Degassed samples

were obtained by bubbling nitrogen through the cuvettes for 30–40 min. Circular dichroism experiments were carried out on a Jasco J-810 spectropolarimeter using 1 cm path length quartz cuvettes. Surface plasmon resonance studies were carried out on a Reichert SR7500DC surface plasmon resonance (SPR) system at 15 °C. Microwave reactions were performed in a CEM Discovery SP Microwave under open vessel conditions unless otherwise stated.

Synthetic Procedures. *4,4'-Di(5-lipoamido-1-pentoxy)-2,2'-bipyridine (bpvSS).* A solution of α-lipoic acid (0.48 g, 2.3 mmol) and 1-hydroxybenzotriazole hydrate (0.36 g, 2.7 mmol) in dry DMF (8.8 mL) was cooled to 0–5 °C, upon which 1-ethyl-3-(3-(dimethylamino)propyl)carbodiimide (EDC) (0.41 g, 2.6 mmol) was added and stirred, maintaining this temperature until the EDC had fully dissolved (ca. 1 h). The solution was allowed to warm to room temperature and stirred for a further hour. A solution of *N*-ethylmorpholine (0.27 g, 2.4 mmol) and 6 (0.35 g, 9.8 mmol) in dry DMF (12.3 mL) was added to the reaction mixture and stirred overnight. The resulting cream precipitate was filtered, dried in air, triturated in CHCl₃ (150 mL), and isolated by filtration, following washings with CHCl₃ (2 × 10 mL) (0.41 g, 39%). Found: C, 58.9; H, 7.1; N, 7.7. Calc. for C₃₆H₅₄N₄O₄S₄: C, 58.8; H, 7.4; N, 7.6%. δ_H (300 MHz; CDCl₃) 1.35–1.65 (12 H, m, H-8,9,15), 1.61–1.78 (8 H, m, H-14,16), 1.79–1.96 (6 H, m, H-10, H-18'), 2.17 (4 H, t, J = 7.4, H-13), 2.38–2.50 (2 H, dddd, J = 0.8, 5.6, 6.3, 6.6, H-18), 3.04–3.10 (4 H, m, H-19), 3.20 (4 H, tt, J = 6.1, 6.7, H-11), 3.50–3.61 (2 H, tdd, J = 1.5, 6.5, 6.5, H-17), 4.13 (4 H, t, J = 6.3, H-7), 5.48 (2 H, br s, NH), 6.82 (2 H, dd, J = 5.7, 2.5, H-5), 7.95 (2 H, d, J = 2.5, H-3) and 8.45 (2 H, d, J = 5.7, H-6); δ_C (100 MHz; CDCl₃) 23.4 (C-9), 25.4 (C-14), 28.6 (C-15), 28.9 (C-8), 29.4 (C-10), 34.6 (C-16), 36.5 (C-13), 38.5 (C-19), 39.3 (C-11), 40.2 (C-18), 56.4 (C-17), 67.7 (C-7), 106.8 (C-3), 111.3 (C-5), 150.2 (C-6), 157.8 (C-2), 166.1 (C-4), and 172.7 (C-12); MS (ESI⁺) *m/z*: 757 (M + Na)⁺. NMR assignments were confirmed by COSY, HSQC, and HMBC.

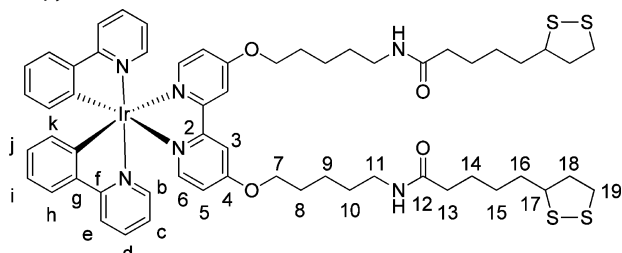
RubySS.



RubpySS was prepared via a modification to a method outlined by Sullivan et al.³⁷ A solution of bpySS (0.19 g, 0.3 mmol) and Ru(bpy)₂Cl₂ (0.13 g, 0.3 mmol) in ethanol (100 mL) was heated under reflux for 16 h. The red/orange solution was cooled to room temperature and concentrated *in vacuo* (~25 mL). H₂O (35 mL) was added, forming a fine cream precipitate, which was filtered. A saturated methanolic solution of ammonium hexafluorophosphate (0.25 g, 1.5 mmol in 2 mL of MeOH) was added to the filtrate to give an orange precipitate. The precipitate was filtered and washed with ice cold H₂O and ice cold Et₂O to give the crude product as an orange/red solid. The solid was dissolved in a minimal amount of acetonitrile and the solvent removed *in vacuo* to give a red crystalline solid RubpySS (0.14 g, 65%). Found: C, 47.2; H, 4.8; N, 7.6. Calc. for C₅₆H₇₀N₈O₄RuS₄(CH₃CN)_{0.25}: C, 46.8; H, 4.9; N, 7.8%. λ_{max} (MeCN)/nm ($\epsilon/\text{dm}^3 \text{ mol}^{-1} \text{ cm}^{-1}$) 289 (77200) and 461 (14600); δ_{H} (300 MHz; CD₃CN) 1.29–1.65 (16 H, m, H-8,9,15,16), 1.68–1.78 (4 H, m, H-14), 1.80–1.92 (6 H, m, H-10,18'), 2.11 (4 H, t, J = 7.2, H-13), 2.37–2.49 (2 H, dddd, J = 6.3, 6.6, H-18), 3.02–3.15 (4 H, m, H-19), 3.15–3.21 (4 H, dt, J = 6.7, 6.2, H-11), 3.52–3.61 (2 H, tdd, J = 2.6, 6.3, 6.5, H-17), 4.21 (4 H, t, J = 6.5, H-7), 6.40 (2 H, t, J = 5.1, NH), 6.92 (2 H, dd, J = 6.5, 2.7, H-5), 7.43 (2 H, d, J = 6.5, H-6), 7.43 (2 H, ddd, J = 1.3, 5.8, 7.8, H-b/b'), 7.44 (2 H, ddd, J = 1.3, 5.8, 7.8, H-b/b'), 7.73 (2 H, d, J = 5.8, H-a/a'), 7.85 (2 H, d, J = 5.8, H-a/a'), 8.00–8.10 (4 H, dd, J = 1.3, 7.8, H-c,c'), 8.07 (2 H, d, J = 2.7, H-3), and 8.47–8.53 (4 H, d, J = 7.8, H-d,d'); δ_{C} (100 MHz; CD₃CN) 22.6 (C-9), 25.2 (C-4), 27.8 (C-15), 28.4 (C-8), 28.9 (C-10), 34.2 (C-16), 35.6 (C-13), 38.1 (C-19), 38.2 (C-11), 40.0 (C-18), 56.4 (C-17), 69.6 (C-7), 111.3 (C-3), 114.1 (C-5), 124.0 (C-d,d'), 127.3 (C-b,b'), 137.2 (C-c,c'), 151.5 (C-a/a'), 151.7 (C-a/a'), 151.9 (C-6), 157.1 (C-2/e,e'), 157.2 (C-2/e,e'), and 166.6 (C-12); MS (ESI⁺) *m/z*: 1294 (M-PF₆)⁺, 574 (M-2(PF₆))²⁺. NMR assignments were confirmed by COSY, HSQC, and HMBC.

Os bpySS. Os bpySS was prepared in a modification to the method outlined by Gaudiello et al.³⁸ Os(bpy)₂Cl₂ (21.8 mg, 0.04 mmol) and bpySS (26.6 mg, 0.04 mmol) were suspended in degassed ethylene glycol (30 mL) and heated under microwave conditions (power = 300 W, *T* = 250 °C) for 7 min. The green/brown mixture was allowed to cool to room temperature, upon which saturated aqueous ammonium hexafluorophosphate (50 mL) was added. The black precipitate was filtered and washed with copious amounts of H₂O and Et₂O, dissolved in a minimal amount of acetone and the solvent removed *in vacuo* to give a black crystalline solid Os bpySS (47.6 mg, 78%). Found: C, 42.9; H, 4.3; N, 7.3. Calc. for C₅₆H₇₀F₁₂N₈O₄OsP₂S₄(NH₄PF₆)_{0.25}: C, 42.9; H, 4.6; N, 7.4%. λ_{max} (MeCN)/nm ($\epsilon/\text{dm}^3 \text{ mol}^{-1} \text{ cm}^{-1}$) 292 (77300), 334 (13600), 459 (13700), and 487 (13500); δ_{H} (300 MHz; CD₃CN) 1.28–1.61 (16 H, m, H-8,9,15,16), 1.61–1.68 (4 H, m, H-14), 1.74–1.89 (6 H, m, H-10,18'), 2.04–2.12 (4 H, m, H-13), 2.32–2.47 (2 H, dddd, J = 6.1, 6.3, H-18), 2.98–3.04 (4 H, m, H-19), 3.04–3.21 (4 H, td, J = 6.1, 6.8, H-11), 3.49–3.60 (2 H, m, H-17), 4.19 (4 H, t, J = 6.5, H-7), 6.35 (2 H, t, J = 4.8, NH), 6.85 (2 H, dd, J = 6.5, 2.7, H-5), 7.19–7.34 (4 H, ddd, J = 1.3, 5.8, 7.8, H-b,b'), 7.23 (2 H, d, J = 6.5, H-6), 7.61 (2 H, d, J = 5.8, H-a/a'), 7.73 (2 H, d, J = 5.8, H-a/a'), 7.79 (4 H, dd, J = 7.8, 1.3, H-c,c'), 8.00 (2 H, d, J = 2.7, H-3), and 8.43 (4 H, t, J = 6.8, H-d,d'); δ_{C} (100 MHz; CD₃CN) 22.3 (C-9), 24.9 (C-4), 27.6 (C-15), 28.2 (C-8), 28.6 (C-10), 34.0 (C-16), 35.3 (C-13), 38.0 (C-11,19), 39.8 (C-18), 56.1 (C-17), 69.4 (C-7), 111.2 (C-3), 114.2 (C-5), 123.9 (C-d,d'), 127.6 (C-b,b'), 136.2 (C-c,c'), 150.2 (C-6/a/a'), 150.6 (C-6/a/a'), 150.9 (C-6/a/a'), 159.0 (C-2/e,e'), 159.3 (C-2/e,e'), and 165.9 (C-12); MS (ESI⁺) *m/z*: 1383 (M-PF₆)⁺. NMR assignments were confirmed by COSY, HSQC, and HMBC.

IrbpySS.



IrbpySS was synthesized via a modified method outlined by Slinker et al.³⁹ [Ir(ppy)₂Cl]₂ (66.6 mg, 0.06 mmol) and bpySS (100.8 mg,

0.14 mmol) was suspended in ethylene glycol (6.5 mL) and heated to 150 °C for 19 h. The yellow mixture was allowed to cool to room temperature, upon which H₂O (150 mL) was added, and the mixture heated to 60–70 °C. Saturated aqueous ammonium hexafluorophosphate (1 g in 2.5 mL H₂O) was added, immediately forming a yellow precipitate, which was cooled on ice, filtered, and washed with H₂O. The solid was dissolved in minimal acetone and the solvent removed *in vacuo* to give IrbpySS (103.8 mg, 61%). Found: C, 50.4; H, 5.5; N, 5.9. Calc. for C₅₈H₇₀F₆IrN₆PS₄: C, 50.5; H, 5.1; N, 6.1%. λ_{max} (MeCN)/nm ($\epsilon/\text{dm}^3 \text{ mol}^{-1} \text{ cm}^{-1}$) 224 (44800), 255 (50000), and 342sh (8200); δ_{H} (300 MHz; acetone-*d*₆) 1.21–1.50 (16 H, m, H-8,9,15,16), 1.50–1.61 (4 H, m, H-14), 1.66–1.81 (6 H, m, H-10,18'), 2.01 (4 H, t, J = 7.1, H-13), 2.25–2.38 (2 H, dddd, J = 0.9, 5.9, 6.3, 6.7, H-18), 2.90–3.05 (8 H, m, H-19), 3.09 (4 H, td, J = 6.5, 6.0), 3.37–3.47 (2 H, m, H-17), 4.17 (4 H, t, J = 6.4, H-7), 6.21 (2 H, d, J = 7.6, H-k), 6.75 (2 H, td, J = 1.3, 7.5, H-j), 6.88 (2 H, td, J = 1.3, 7.5, H-i), 6.95 (2 H, t, J = 5.5, NH), 7.06 (2 H, dd, J = 1.3, 5.8, H-d), 7.08 (2 H, dd, J = 2.5, H-5), 7.69 (2 H, d, J = 6.4, H-6), 7.72–7.78 (4 H, m, H-e,h), 7.83 (2 H, dd, J = 1.3, 8.0, H-c), 8.10 (2 H, d, J = 8.0, H-b), and 8.29 (2 H, d, J = 2.5, H-3); δ_{C} (100 MHz; acetone-*d*₆) 23.7 (C-9), 26.3 (C-4), 28.9 (C-15), 29.3–30.4 (C-8, masked by NMR solvent), 35.4 (C-16), 36.6 (C-13), 39.1 (C-19), 39.2 (C-11), 41.0 (C-18), 57.3 (C-17), 70.4 (C-7), 112.7 (C-6), 115.2 (C-5/d), 120.6 (C-b), 123.1 (C-j), 124.4 (C-5/d), 125.8 (C-3/k), 131.1 (C-i), 132.6 (C-h), 139.3 (C-c), 145.0 (C-f), 152.0 (C-g), 152.3 (C-3/k), 154.2 (C-e), 158.5 (C-2), 168.3 (C-4), 168.8 (C-a), and 172.8 (C-12); MS (ESI⁺) *m/z*: 1235 (M-PF₆)⁺. NMR assignments were confirmed by COSY, HSQC, and HMBC.

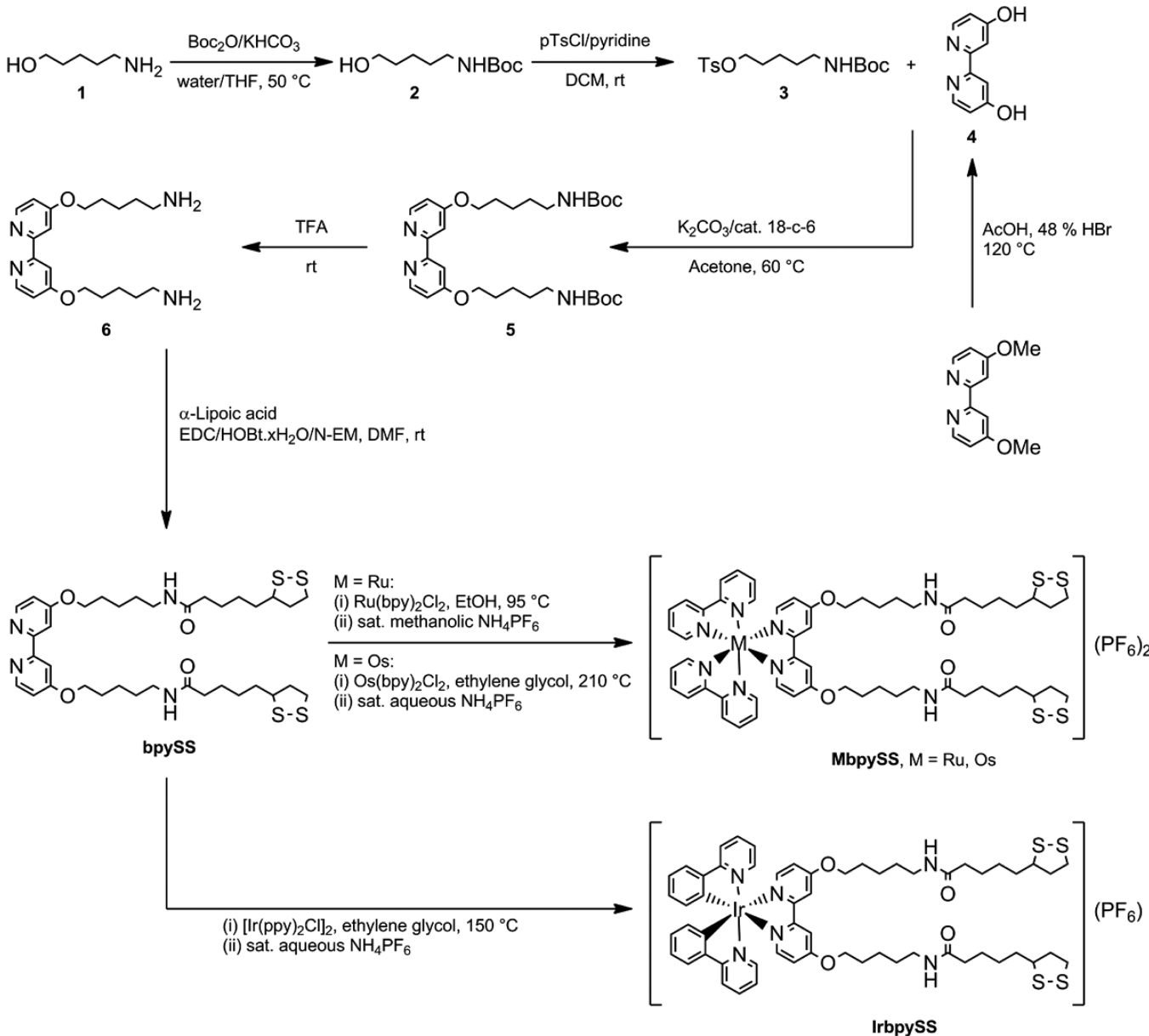
Surface Preparation. Gold substrates were cleaned using a UVO cleaner (1 h) and immersed in MeCN for at least 10 min before use. Slides were immersed in a 1 mM solution of complex and 2 mM TCEP-HCl (1:1 MeCN/H₂O) and sealed from the outside atmosphere to prevent solvent evaporation. The slides were left immersed for a stipulated amount of time, before immersion in clean MeCN and drying under N₂.

Micropatterning Surface via the Micro-Contact Printing Method. Gold slides were cleaned by the general method described above. Stamps were made as per the method outlined by Whitesides et al.⁴⁰ from PDMS. PDMS/PDMS curing agent (9:1) was mixed for 10 min and poured onto the masters. The mixture was allowed to cure at room temperature for 1 h, and the bubbles that formed on the top of the mixture were removed manually. The mixture was then cured in the oven at 60 °C for 1 h. The PDMS stamps were peeled away from the masters and cut into shape. The stamps were then oxidized by UVO cleaner (1 h) and immersed in MeCN for 10 min. The stamps with inked by immersion in a 5 mM solution of complex and 10 mM TCEP-HCl (1:1 MeCN/H₂O) for 30 min before drying under N₂. The stamps were placed firmly (with the aid of a small weight) on the clean gold slides (~12 kPa) for 16 h before peeling the stamp away to leave the micropatterned surface. The slides were then washed by immersion in clean MeCN and dried under N₂.

Procedure for SPR Studies. Gold chips (50 nm on glass, Reichert) were cleaned in Piranha solution (CAUTION: Piranha solution reacts violently with organic material) for 10 min, washed with ultrahigh purity (UHQ 18 MΩ cm) water followed by ethanol, and stored in ethanol until used. During the experiments, the chips were equilibrated in the solvent system used for each experiment for at least 10 min to ensure a steady baseline. The system was then injected with the appropriate solution at an initial flow rate of 1500 μL min⁻¹ followed by a flow rate of 10 or 0 μL min⁻¹. The slides were then washed with the solvent system at a flow rate of 1500 μL min⁻¹.

X-ray photoelectron spectroscopy was carried out at the University of Leeds by Dr. Benjamin Johnson. The instrument is a VG ESCALab 250 with a monochromated Al K α source. Experiments were performed in UHV (~10⁻¹⁰ mbar). Survey scans were recorded at a pass energy of 150 eV, detailed scans at 20 eV. Offline analysis of the spectra was performed using Casa 2.3.15 XPS software.

Scheme 2. Synthetic Route for Preparation of RubpySS, IrbpySS, and OsbpySS



RESULTS AND DISCUSSION

Synthesis. The ligand explored in this study was synthesized by appending 5-amino-1-pentanol ‘legs’ to dihydroxy-2,2'-bipyridine, followed by an amide coupling with α -lipoic acid to yield the surface-active bpySS ligand (Scheme 2).

The ruthenium(II) and osmium(II) complexes were synthesized by reaction of $\text{M}(\text{bpy})_2\text{Cl}_2$ ($\text{M} = \text{Ru, Os}$) with the bpySS ligand followed by precipitation with NH_4PF_6 (Scheme 2). The cyclometalated iridium(III) complex was synthesized via reaction of the bpySS ligand with $[\text{Ir}(\text{ppy})_2\text{Cl}]_2$, followed by precipitation with NH_4PF_6 . All complexes were synthesized with acceptable (60–80%) yields and fully characterized by ^1H and ^{13}C NMR spectroscopy, mass spectrometry, elemental analysis, and UV-visible absorption spectroscopy (Supporting Information).

Photophysical Properties of RubpySS, IrbpySS, and OsbpySS in Solution. The absorption and luminescence properties of the complexes are summarized in Table 1. The absorption spectrum of RubpySS shows two characteristic absorption

bands at 289 and 461 nm, corresponding to the ${}^1(\pi-\pi^*)$ and singlet metal-to-ligand charge transfer (${}^1\text{MLCT}$) bands, respectively (Supporting Information). OsbpySS has a similar absorption spectrum, with two absorption bands at 292 and 487 nm, in agreement with similar osmium(II) complexes.^{41–43} It is noteworthy that the ${}^1\text{MLCT}$ bands of RubpySS and OsbpySS are red-shifted by 9 and 5 nm, respectively, compared to tris-bipyridyl analogues of each of the complexes, in agreement with other complexes with 4,4'-disubstituted bipyridine ligands with electron donating substituents, as evidenced by 4,4'-dimethoxy bipyridyl ruthenium(II) complexes.^{41,44,45} The absorption spectrum of IrbpySS shows a peak in the UV region, centered at 255 nm, in agreement with other iridium(III) complexes with functionalized bipyridyl ligands.^{46,47} The luminescence properties of the complexes are summarized in Table 1. IrbpySS has the highest energy emission state, with an emission maximum at 580 nm, comparable to similar iridium(III) complexes,^{15,39,48} originating from significant mixing between the ${}^3\pi-\pi^*$, ${}^1\text{MLCT}$, and ${}^3\text{MLCT}$ states due to spin-orbit coupling.^{35,39,49} The luminescence spectra

Table 1. Absorption and Luminescence Properties of Metal Complexes

complex	$\lambda_{\text{max}}/\text{nm}$ ($\epsilon/10^4 \text{ M}^{-1} \text{ cm}^{-1}$)	$\lambda_{\text{em}}/\text{nm}$	τ/ns		$\Phi/\%$	
			aerated	deaeerated	aerated	deaeerated
RubpySS	289 (7.8), 323 (1.3), 461 (1.5)	645	130	707	1	4
OsbpySS	292 (7.7), 317 (1.3), 487 (1.4)	790	20	25	0.1	0.1
IrbpySS	255 (5.0), 298 (1.8) sh, 337 (0.8) sh	580	25 (68%) 80 (32%)	35 (34%) 246 (66%)	0.5	3
[Ru(bpy) ₃]Cl ₂	452 (1.3) ⁵⁴	615 ⁵⁴	172	840	1	10
[Ost(bpy) ₃](PF ₆) ₂	482 (1.1)	723	39	58	0.3	0.5
[Ir(ppy) ₂ (dtb-bpy)](PF ₆) ^a		580 ³⁹	65 ³⁹	557 ³⁹		24 ³⁹

^adtb-bpy = 4,4'-di-*tert*-butyl-2,2'-bipyridine.

of RubpySS and OsbpySS show ³MLCT based broad emission centered at 645 and 790 nm, respectively. Both spectra are significantly red-shifted from their tris-bipyridyl analogues (30 and 67 nm, respectively), suggesting that the bulky moieties have a stabilizing effect on the excited state, in agreement with other similar ruthenium(II) and osmium(II) complexes.^{44,45,50,51} The range of emission profiles of the three complexes, from the yellow of iridium to the far red of ruthenium and osmium, implies their usefulness in participating as donor/acceptor photoactive units (Figure 1) in

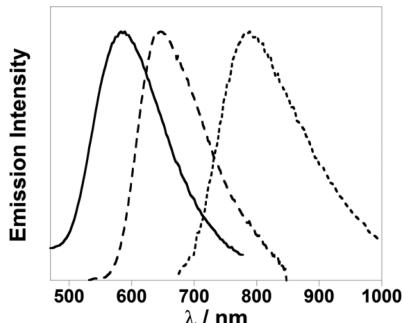


Figure 1. Photoluminescence emission spectra of IrbpySS (solid line, $\lambda_{\text{exc}} = 280 \text{ nm}$), RubpySS (long dash line, $\lambda_{\text{exc}} = 465 \text{ nm}$), and OsbpySS (short dash line, $\lambda_{\text{exc}} = 491 \text{ nm}$) in acetonitrile solutions. Spectra corrected for instruction response for detection. Intensities are not to scale.

energy cascades, as has been reported previously for supramolecular systems.^{52,53} The complexes possess lifetimes characteristic of the nature of their excited states. The longer lifetimes of RubpySS and IrbpySS solutions in deaeerated conditions demonstrate the extent of ³O₂ quenching of their excited states.

Immobilization of RubpySS, IrbpySS, and OsbpySS on Gold Surfaces. To study the surface attachment of the metal complexes on gold, ellipsometric, surface plasmon resonance, and X-ray photoelectron spectroscopy (XPS) studies were carried out. Surfaces were treated with aqueous acetonitrile (1:1) solutions of the complexes with two equivalents of a reducing agent, *tris*-(2-carboxyethyl)phosphine hydrochloride (TCEPH⁺Cl⁻) added to aid the reduction of the disulfide attachments. The time-resolved ellipsometric plots of monolayer formation on gold for RubpySS and IrbpySS show an increase in layer thickness over a period of 10 min, with full coverage achieved within 30 min (Figure 2a,b). A 24 h study confirms the stability of the RubpySS-Au monolayer (Supporting Information). The layer thickness at 30 min is $1.8 \pm 0.1 \text{ nm}$ for RubpySS-Au and $1.7 \pm 0.1 \text{ nm}$ for IrbpySS-Au. These values were compared with simplified models of the height of the complexes on planar surfaces, at a tilt angle of 40° reported for lipoic acid⁵⁵ (Figure 2d) and were found to be in good agreement (ca. 2 nm) with the

experimental values obtained. These results also agree well with ellipsometric results from the growth of a palladium film formed by a layer-by-layer method.⁵⁶

Surface plasmon resonance (SPR) spectroscopy studies were performed to examine the formation of monolayers of RubpySS·Au and IrbpySS·Au on gold substrates. SPR studies measure a change in refractive index, which is calculated from the angle of minimum intensity from a light source which is shined at a prism on the back of a gold sensor chip. This change in refractive index at the surface is due to adsorbates coming into proximity with the surface of the sensor chip. For larger adsorbates such as proteins, this change is generally high (ca. 0.4° or 4000 μRIU where RIU = refractive index unit),^{57–59} with smaller adsorbates expected to have lower responses, as molecular weight can contribute to the response.⁶⁰ Adsorption kinetics for adsorbates with molecular weights as low as hexadecanethiol have been previously studied.⁶¹ The solid lines (Figure 2c) show the kinetics of adsorption of a 1 mM RubpySS or IrbpySS solution in 1:1 acetonitrile/water. For RubpySS, we observe an increase in response units over 30 min from 0 to 0.30°, showing an association of the complex with the substrate. Subsequent washing in clean 1:1 acetonitrile/water at a flow rate of 1500 μL min⁻¹ followed by 10 min at a flow rate of 50 μL min⁻¹ shows that some complex is specifically adsorbed to the surface, with an average response of 0.20° even after solvent wash, which we expect for smaller adsorbates.⁶¹ A similar trend is observed for IrbpySS, with the response increasing over 30 min from 0 to 0.37°. Following the wash step, the signal drops to 0.31°, also indicative of specific binding to the gold substrate. Control studies were also conducted, examining any possible adsorption of reducing agent or solvent effect (Figure 2c). The TCEPH⁺Cl⁻ control shows that there is some association during the course of the experiment, but it is only nonspecifically adsorbed, with all of the reducing agent being removed to leave 0.05° following a wash in clean solvent. The clean solvent control also shows negligible adsorption (0.05°) to the substrate within experimental error. These results confirm the stability of the monolayer as shown in the ellipsometric studies, with the same final response units recorded for RubpySS·Au (ca. 0.19°) after 30 min or 24 h (Supporting Information).

XPS analysis of the RubpySS·Au and IrbpySS·Au monolayers reveals the presence of each of the elements present in the complexes on gold. The Ru 3d_{5/2} and 3d_{3/2} photoelectron peaks present at 281.1 and 286.1 eV, respectively, while the Ir 4f_{7/2} and 4f_{5/2} peaks appear at 61.8 and 64.8 eV, respectively (Supporting Information). The RubpySS·Au monolayer was examined under two preparation routes, with and without treatment using TCEPH⁺Cl⁻. The S 2p region of the spectrum of the monolayer RubpySS·Au without the TCEPH⁺Cl⁻ treatment shows only two environments, with S 2p_{3/2} peaks at 161.6 and 163.1 eV corresponding to thiolate (66%) and disulfide (34%), respectively, previously assigned for thioctic acid monolayers.⁵⁵ A monolayer of RubpySS·Au treated with TCEPH⁺Cl⁻ also

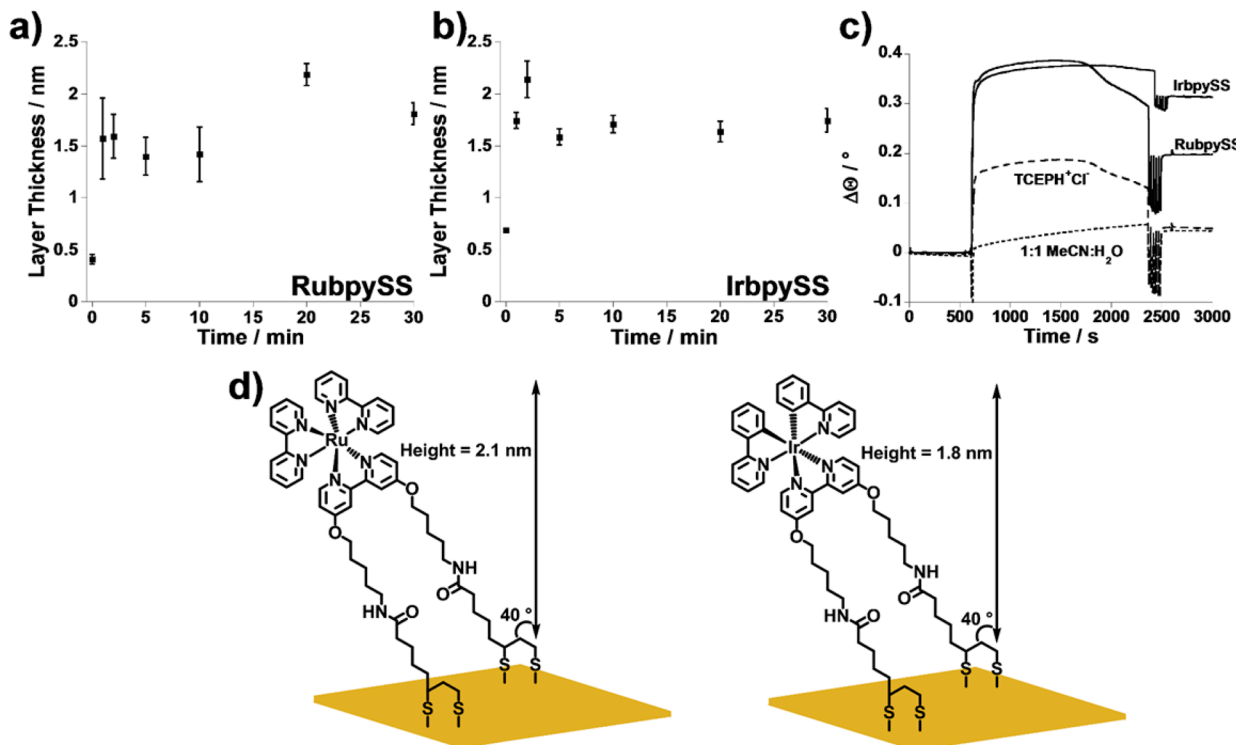


Figure 2. Plot of ellipsometric data for time dependence of monolayer formation of (a) RubpySS and (b) IrbpySS. (c) SPR sensorgram to monitor monolayer formation of IrbpySS (1 mM), RubpySS (1 mM), control solution ($\text{TCEPH}^+\text{Cl}^-$), dotted line (2 mM), and solvent control (1:1, $\text{H}_2\text{O}/\text{CH}_3\text{CN}$) on a gold substrate over 30 min. Solutions were injected across clean gold surfaces. (d) Schematic of RubpySS·Au and IrbpySS·Au adhered to gold substrates.

shows only two environments at the same peak positions with a thiolate (75%) and disulfide (25%), respectively (Figure 3).

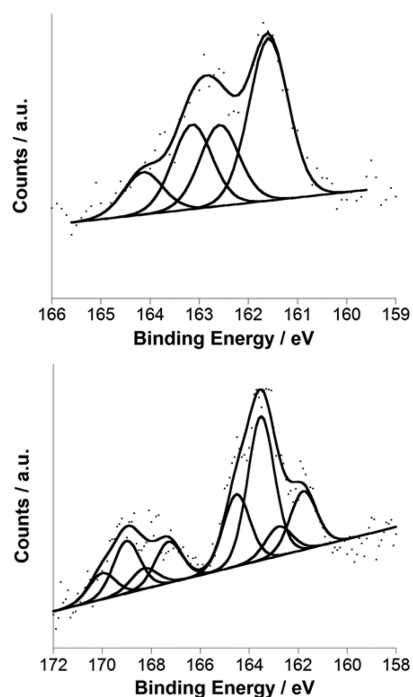


Figure 3. XPS S 2p spectra of RubpySS·Au (top) and IrbpySS·Au (bottom). Recorded spectra (dots) are fitted with linear backgrounds and show curve fitting components (solid lines).

These results show that the great majority of the disulfide anchors are reduced to thiolate to bind to gold and that the

treatment with the reducing agent has a small effect on thiolate formation. The estimated Ru/S ratio from the peaks is 1:4 which is in agreement with the molecular formula of the complex.

The S 2p region of the spectrum of the IrbpySS·Au reveals the S $2p_{3/2}$ peaks at 161.8 and 163.5 eV with an additional peak identified as oxidized sulfur between 167 and 169 eV (Figure 3). The peaks at 161.8 and 163.5 eV are assigned to thiolate and disulfide species as previously reported.⁵⁵ The peak of the oxidized species is usually attributed to sulfonate; the peak can be fitted to two environments at 167.3 and 169.0 eV.⁶² For this monolayer, 48% of the overall sulfur region exists in the disulfide form. The oxidized species account for 32% of the total sulfur. The peaks for C 1s, N 1s, and O 1s for both complexes were also observed. The formation of oxidized species has been observed previously⁶² and has been shown to be eliminated by longer monolayer assembly times. Although the difference of the binding mode of the anchoring group in RubpySS·Au and IrbpySS·Au monolayers is not apparently linked to the preparation method, it is clear that in both cases the metal complex is bound to the gold surface.

Monolayer samples of RubpySS·Au and IrbpySS·Au display the characteristic charge transfer based emission at 630 and 532 nm, respectively (Figure 4). Blue-shifts of 15 and 48 nm for RubpySS·Au and IrbpySS·Au occur, respectively, from the solution spectra. A similar trend is also observed for the powder spectra of RubpySS and IrbpySS, with blue-shifts of 4 and 26 nm from the solution spectra, respectively. Neat solid iridium(III) complexes with blue-shifts similar to that observed in acetonitrile solutions have been previously reported,¹⁵ as have those for similar ruthenium(II) complexes.⁶³ For the case of ruthenium(II) complexes, these shifts are attributed to the lack of solvent influence in the stabilization of the charge transfer states and

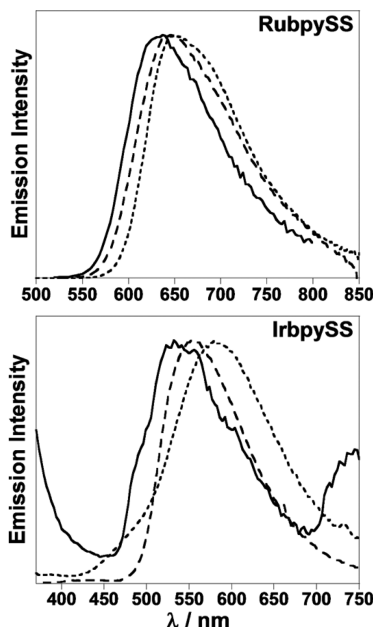


Figure 4. Overlays of luminescence spectra of RubpySS (top), $\lambda_{\text{exc}} = 465 \text{ nm}$, and IrbpySS (bottom), $\lambda_{\text{exc}} = 360 \text{ nm}$; monolayer (solid line), powder (long dash line), and solution in acetonitrile (short dash line). Emission spectra corrected for instrument response for detection. Intensities are not to scale.

possibly the effect of lack of free movement of the complexes. The blue shifts on the surface indicate the influence of the anchoring to the substrate, resulting in a reduction in vibronic coupling associated with excited states in the solution and thus leading to a tightening of the excited state bands which renders the transition higher in energy. The excitation spectra show similar λ_{max} values to those of solution samples, with no discernible shifts in the bands of the spectra. OsbpySS·Au monolayers on gold surfaces were also prepared; however, luminescence from these surfaces was too weak to detect.

The luminescence lifetime of the RubpySS·Au monolayer is 210 ns (Table 2), which is considerably longer than the aerated solution (130 ns), and comparable to the powder (200 ns). This enhancement of lifetime is in contrast to previous studies that quenching of ruthenium(II) emission was observed when at small distances (within ca. 10 nm) of the surface.^{23,64} The luminescence lifetime of IrbpySS·Au on the surface was calculated to be biexponential, with a long component of 130 ns (83%) and a short component of 12 ns (17%). These lifetimes are longer than those calculated in aerated solution (25, 80 ns) and again comparable to that of the powder (110, 30 ns). These results suggest that not only is there no quenching from the gold surface but also there is enhancement of luminescence compared with solutions of the complexes. The luminescence signal is also strong enough to allow luminescence microscopy images of the monolayers of the complexes to be collected (Supporting Information).

To demonstrate the usefulness of transition-metal complex systems in lab-on-chip opto-responsive devices, we used the microcontact printing method outlined by the group of Whitesides.⁴⁰ Such formed stamps from transition metal complexes can be used in sensing applications if the metal complex is firmly attached to the surface and does not wash away during cleaning steps designed to remove unbound complexes.

Poly(dimethylsiloxane) (PDMS) stamps patterned with 10 μm -wide inking areas were inked with 5 mM RubpySS or IrbpySS and 10 mM TCEPH⁺Cl⁻ for 30 min by immersion in a 1:1 acetonitrile/water solution, followed by drying and stamping

Table 2. Photoluminescence Data for Interaction of Complexes with 10 Mol Equiv of BSA^a

complex	τ/ns	
	before BSA addition	after BSA addition
RubySS in 0.5% CH ₃ CN in water	210	84 (4%), 250 (96%)
IrbpySS in 0.5% CH ₃ CN in water	15	37 (8%), 283 (92%)
[Ru(bpy) ₃] ²⁺ in 0.5% CH ₃ CN in water	393	387
RubySS·Au surface	210	283
IrbpySS·Au surface	12 (17%), 130 (83%)	15 (30%), 170 (70%)

^aConcentrations of complexes, ca. 1 μM . Surfaces immersed in 15 μM solution of BSA for 30 min.

for 16 h. Luminescence microscopy of the patterned surfaces shows emission from ruthenium iridium(III) complexes, revealing that the patterning was successful. In the image of the RubpySS·Au pattern (Figure 5), the lines show brighter spots

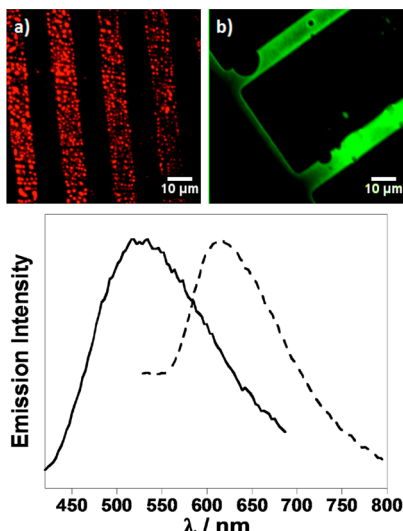


Figure 5. (Top) Luminescence microscope images of patterned complexes on gold substrates. (a) RubpySS·Au; (b) IrbpySS·Au. (Bottom) Steady state emission spectra of stamped surfaces. Solid line, IrbpySS·Au; dashed line, RubpySS·Au. Spectra corrected for instrument response for detection. Intensities are not to scale.

that may originate from the stamping process or the quality of the features of the stamp. The image of stamped IrbpySS (Figure 5) reveals the 10 μm wide areas and illustrates that many patterns can be utilized in order to create functional devices. Luminescence spectroscopy studies (Figure 5) of the patterned complexes confirm the distinct ³MLCT emission from the ruthenium(II) center and emission from the iridium(III) center.

We noted that, in order to create more robust patterns, the stamping time is considerably longer than those of simple alkanethiols. Luminescence microscopy of different substrates with stamping times up to 2 h often led to most or all of the complex being removed from the surface during the washing stage. We speculate that this could be due to lipophilic interactions with the legs of the complexes due to the innately higher concentrations of complex at the stamp surface that inhibits the gold–thiolate interaction. We believe that this observation also contributes to some defect formation in the finished patterns, as shown by the round defects in the IrbpySS pattern.

Biomolecular Recognition Studies on Surfaces and in Solution. The interaction of the modified gold monolayers

RubpySS·Au and IrpySS·Au with bovine serum albumin (BSA) was studied by SPR and luminescence spectroscopy, accompanied by solution steady state and time-resolved emission spectroscopy, as well as circular dichroism spectroscopy. To monitor the changes on the gold surfaces upon BSA addition, we employed SPR studies. A solution of BSA (15 μM in water) was added to monolayers of RubpySS·Au and IrpySS·Au, and the SPR response was recorded (Figure 6). A large change in $\Delta\Theta$ was

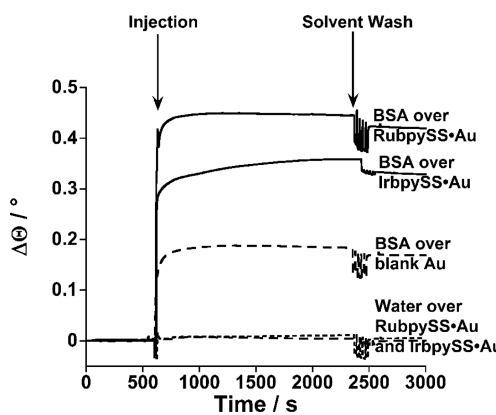


Figure 6. SPR sensograms of BSA injected across monolayers of RubpySS·Au or IrpySS·Au (solid line), BSA injected across a blank gold substrate (long dash line), and a blank solution of water injected across a monolayer of RubpySS·Au or IrpySS·Au (short dash line).

observed for both surfaces upon introduction of BSA, displaying an increase of more than double the interaction of BSA with clean gold surfaces. We speculate that this affinity is most likely due to two possible factors, (a) hydrophobic interactions in the binding pockets of BSA, such as fatty acid binding sites III and IV, which can change shape and accommodate up to six fatty acid chains through nonpolar interactions^{65,66} and (b) Coulombic interactions through an increase of the net positive charge at the surface. Upon injection of water across monolayers of RubpySS·Au and IrpySS·Au used as a control study, we observe no increase in response, confirming that the change in response is only due to specific adsorption of BSA molecules.

The interaction of the BSA was also studied by the change in the environment of the metal complex using luminescence lifetime measurements. Addition of a solution of BSA (15 μM in water) to RubpySS·Au and IrpySS·Au monolayers was monitored by the luminescence lifetime decays (Table 2). Upon interaction with BSA, we observe a luminescence lifetime increase for IrpySS·Au monolayers, with the major component increased from 130 to 170 ns, indicating that interactions between the complex and BSA occur when anchored to gold substrates. This change is expected on the basis of charge transfer state character of the complex, which is sensitive to changes in the environment and consequently to interactions with BSA. In solution experiments, where 10 mol equiv of BSA was added to ca. 1 μM solutions of IrpySS or RubpySS, a similar trend is observed for IrpySS, with an increase in luminescence lifetime from 15 ns to 37 and 283 ns. Similar results for iridium(III) complexes have also been reported where binding occurs through hydrophobic chains and indole moieties specific to the binding of BSA that lead to increased lifetimes and emission intensities due to the increased hydrophobicity of the iridium(III) environment.⁶⁷ The lifetime of RubpySS·Au monolayers increased from 210 to 283 ns upon immersion in BSA solutions, and a change in solution experiments also indicated some bind-

ing, with the lifetime changing from monoexponential in solution (210 ns) to biexponential upon addition of BSA (84, 250 ns) (Table 2). No observable change in luminescence lifetime was observed when solution samples of the control complex [Ru(bpy)₃]Cl₂ were examined (Table 2).

To monitor the interaction of the metal complexes with BSA in solutions independently, we studied the effect of BSA addition to the luminescence signal of the metal complex. Solutions of IrpySS displayed a large 80-fold increase in the integrated emission intensity signal corrected for BSA absorption at 350 nm (Figure 7) with a concurrent 13 nm blue shift. The luminescence

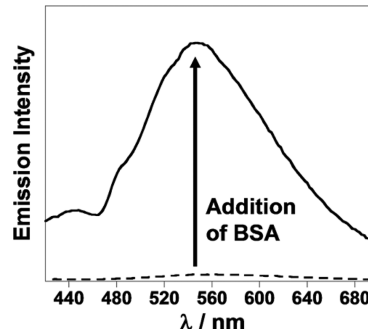


Figure 7. Steady state emission spectra of IrpySS (0.7 μM) solution before (long dash line) and after (solid line) BSA (15 μM) addition. Spectra corrected for instrument response for detection. $\lambda_{\text{exc}} = 350$ nm.

signal of RubpySS was less affected; a 90% increase was observed upon BSA addition. The signal of complex [Ru(bpy)₃]Cl₂ changed only by 30%.

To further demonstrate the biomolecular interactions in solution, circular dichroism spectroscopy was employed. The spectra (Figure 8) show the presence of BSA, with two negative

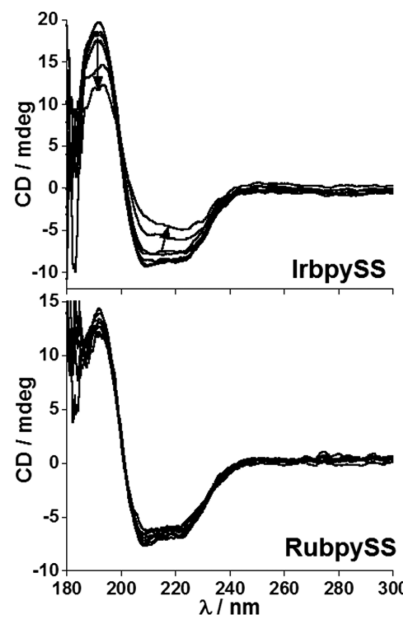


Figure 8. Circular dichroism spectra of BSA (0.1 μM) with the additions of IrpySS (100 μM) (top) in 0.1, 0.4, 0.8, 4.1, 8.2, 41.0, and 82.2 equiv and RubpySS (100 μM) (bottom) in 0.1, 0.4, 0.8, 4.0, 8.1, 40.5, and 81.0 equiv.

peaks at 209 and 222 nm, as well as a positive peak at 190 nm.⁶⁸ Upon the sequential addition of a solution of IrpySS (10 μM), a

decrease in intensity of these peaks is observed, indicating change on the structural features of the protein, attributed to interaction with Ir(bpy)SS. In contrast, we see no interaction between BSA and RubpySS (Figure 8) or $[\text{Ru}(\text{bpy})_3]^{2+}$ (Supporting Information). We speculate that the stronger interaction of Ir(bpy)SS is assisted by the more hydrophobic nature of iridium increasing the hydrophobic interactions with BSA and allowing the complex to bind into a cavity, changing the secondary structure of the BSA.

CONCLUSIONS

We have presented three novel luminescent transition metal complexes with surface-active moieties designed to attenuate quenching associated with luminescent thin films on planar metal surfaces. The results show that not only is quenching reduced but also the luminescence lifetimes of the complexes are enhanced when the complexes are anchored to gold surfaces. We have shown that complexes of this type can be patterned directly using a simple stamping methodology and explored the possibility of multimodal sensing applications of these surfaces using SPR and luminescence studies in the detection of bovine serum albumin. The iridium(III) monolayers show the most sensitive response upon protein binding based on luminescence detection, and they can also be used for sensing by SPR, proving the concept of multimodal detection. Future studies will invariably be focused on improving these systems with novel designs for the remaining bipyridine/phenylpyridine ligands to create complexes with specific sensing properties for antibodies and other biomolecules. The stability of these complexes to stamping makes the methodology attractive for developing surfaces in optoelectronic lab-on-chip devices, that incorporate flow systems or other platforms in which luminescence can be introduced as a very sensitive detection method together with SPR. Luminescence imaging can provide very sensitive detection in lab-on-chip devices for multianalyte binding fabricated with microcontact printing methods.

ASSOCIATED CONTENT

Supporting Information

Synthetic methodology of the reactions for preparation of the ligand, 2D NMR and UV-vis spectra of the complexes, additional circular dichroism spectra, control ellipsometry data, and further XPS spectra showing all the regions. This material is available free of charge via the Internet at <http://pubs.acs.org/>.

AUTHOR INFORMATION

Corresponding Author

*E-mail: z.pikramenou@bham.ac.uk.

Notes

The authors declare no competing financial interest.

ACKNOWLEDGMENTS

The authors would also like to thank Dr. Benjamin Johnson (University of Leeds) and Leeds EPSRC Nanoscience and Nanotechnology Facility (LENNF) for performing and fitting XPS experiments and also Prof. Paula M. Mendes and Dr. Chun Yeung for the provision of silicon masters with which to produce the PDMS stamps used in this work. We acknowledge the EPSRC, The Leverhulme Trust and the School of Chemistry, University of Birmingham for funding. Some of the spectrometers used in this research were obtained through Birmingham Science City: Innovative Uses for Advanced Materials in the

Modern World (West Midlands Centre for Advanced Materials Project 2), with support from Advantage West Midlands (AWM) and partial funding from the European Regional Development Fund (ERDF).

REFERENCES

- (1) Fahrenbach, A. C.; Warren, S. C.; Incorvati, J. T.; Avestro, A.-J.; Barnes, J. C.; Stoddart, J. F.; Grzybowski, B. A. Organic Switches for Surfaces and Devices. *Adv. Mater.* **2013**, *25*, 331–348.
- (2) Puigmarti-Luis, J.; Rubio-Martinez, M.; Imaz, I.; Cvetkovic, B. Z.; Abad, L.; Perez del Pino, A.; Maspoch, D.; Amabilino, D. B. Localized, Stepwise Template Growth of Functional Nanowires from an Amino Acid-Supported Framework in a Microfluidic Chip. *ACS Nano* **2014**, *8*, 818–826.
- (3) Gong, Y.; Yang, S.; Zhan, L.; Ma, L.; Vajtai, R.; Ajayan, P. M. A Bottom-up Approach to Build 3d Architectures from Nanosheets for Superior Lithium Storage. *Adv. Funct. Mater.* **2014**, *24*, 125–130.
- (4) Guo, X.; Ying, Y.; Tong, L. Photonic Nanowires: From Subwavelength Waveguides to Optical Sensors. *Acc. Chem. Res.* **2014**, *47*, 656–666.
- (5) Love, J. C.; Estroff, L. E.; Kriebel, J. K.; Nuzzo, R. G.; Whitesides, G. M. Self-Assembled Monolayers of Thiolates on Metals as a Form of Nanotechnology. *Chem. Rev.* **2005**, *105*, 1103–1169.
- (6) Perl, A.; Reinhoudt, D. N.; Huskens, J. Microcontact Printing: Limitations and Achievements. *Adv. Mater.* **2009**, *21*, 2257–2268.
- (7) Xia, Y.; Rogers, J. A.; Paul, K. E.; Whitesides, G. M. Unconventional Methods for Fabricating and Patterning Nanostructures. *Chem. Rev.* **1999**, *99*, 1823–1848.
- (8) Demming, A.; Osterbacka, P. R.; Han, D. J.-W. Nanotechnology in Paper Electronics. *Nanotechnology* **2014**, *25*, 090201–090201.
- (9) Dorokhin, D.; Hsu, S.-H.; Tomczak, N.; Reinhoudt, D. N.; Huskens, J.; Velders, A. H.; Vancso, G. J. Fabrication and Luminescence of Designer Surface Patterns with beta-Cyclodextrin Functionalized Quantum Dots Via Multivalent Supramolecular Coupling. *ACS Nano* **2010**, *4*, 137–142.
- (10) Basabe-Desmonts, L.; Reinhoudt, D. N.; Crego-Calama, M. Design of Fluorescent Materials for Chemical Sensing. *Chem. Soc. Rev.* **2007**, *36*, 993–1017.
- (11) Liebau, M.; Huskens, J.; Reinhoudt, D. N. Microcontact Printing with Heavyweight Inks. *Adv. Funct. Mater.* **2001**, *11*, 147–150.
- (12) Rogers, N.; Claire, S.; Harris, R.; Farabi, S.; Zikeli, G.; Styles, I.; Hodges, N.; Pikramenou, Z. High Coating of Ru(II) Complexes on Gold Nanoparticles for Single Particle Luminescence Imaging in Cells. *Chem. Commun.* **2014**, *50*, 617–619.
- (13) Rapino, S.; Valenti, G.; Marcu, R.; Giorgio, M.; Marcaccio, M.; Paolucci, F. Microdrawing and Highlighting a Reactive Surface. *J. Mater. Chem.* **2010**, *20*, 7272–7275.
- (14) Zanarini, S.; Rampazzo, E.; Della Ciana, L.; Marcaccio, M.; Marzocchi, E.; Montalti, M.; Paolucci, F.; Prodi, L. Ru(bpy)₃ Covalently Doped Silica Nanoparticles as Multicenter Tunable Structures for Electrochemiluminescence Amplification. *J. Am. Chem. Soc.* **2009**, *131*, 2260–2267.
- (15) Tamayo, A. B.; Garon, S.; Sajoto, T.; Djurovich, P. I.; Tsypa, I. M.; Bau, R.; Thompson, M. E. Cationic Bis-Cyclometalated Iridium(III) Diimine Complexes and Their Use in Efficient Blue, Green, and Red Electrochemiluminescent Devices. *Inorg. Chem.* **2005**, *44*, 8723–8732.
- (16) Zhang, J.; Chu, B. W.-K.; Zhu, N.; Yam, V. W.-W. Synthesis, Characterization, Langmuir-Blodgett Film-Forming Property, and Second-Order Nonlinear Optical Study of Rhodium(I) and Ruthenium(II) Diimine Complexes. *Organometallics* **2007**, *26*, 5423–5429.
- (17) Chu, B. W.-K.; Yam, V. W.-W. Sensitive Single-Layered Oxygen-Sensing Systems: Polypyridyl Ruthenium(II) Complexes Covalently Attached or Deposited as Langmuir-Blodgett Monolayer on Glass Surfaces. *Langmuir* **2006**, *22*, 7437–7443.
- (18) Krass, H.; Plummer, E. A.; Haider, J. M.; Barker, P. R.; Alcock, N. W.; Pikramenou, Z.; Hannon, M. J.; Kurth, D. G. Immobilization of Π -Assembled Metallo-Supramolecular Arrays in Thin Films: From

- Crystal-Engineered Structures to Processable Materials. *Angew. Chem., Int. Ed.* **2001**, *40*, 3862–3865.
- (19) Hoertz, P. G.; Mallouk, T. E. Light-to-Chemical Energy Conversion in Lamellar Solids and Thin Films. *Inorg. Chem.* **2005**, *44*, 6828–6840.
- (20) Piper, D. J. E.; Barbante, G. J.; Brack, N.; Pigram, P. J.; Hogan, C. F. Highly Stable Redox Active Films Formed by the Electrografting of a Diazotized Ruthenium Complex Generated *in Situ* from the Amine. *Langmuir* **2011**, *27*, 474–480.
- (21) Zanarini, S.; Rampazzo, E.; Bich, D.; Canteri, R.; Della Ciana, L.; Marcaccio, M.; Marzocchi, E.; Montalti, M.; Panciatichi, C.; Pederzolli, C.; Paolucci, F.; Prodi, L.; Vanzetti, L. Synthesis and Electro-chemiluminescence of a Ru(bpy)₃-Labeled Coupling Adduct Produced on a Self-Assembled Monolayer. *J. Phys. Chem. C* **2008**, *112*, 2949–2957.
- (22) Bayly, S. R.; Gray, T. M.; Chmielewski, M. J.; Davis, J. J.; Beer, P. D. Anion Templated Surface Assembly of a Redox-Active Sensory Rotaxane. *Chem. Commun.* **2007**, 2234–2236.
- (23) Ramachandra, S.; Schuermann, K. C.; Edafe, F.; Belser, P.; Nijhuis, C. A.; Reus, W. F.; Whitesides, G. M.; De Cola, L. Luminescent Ruthenium Tripod Complexes: Properties in Solution and on Conductive Surfaces. *Inorg. Chem.* **2011**, *50*, 1581–1591.
- (24) Contreras-Carballeda, P.; Edafe, F.; Tichelaar, F. D.; Belser, P.; De Cola, L.; Williams, R. M. Tripodal Osmium Polypyridyl Complexes for Self-Assembly on Platinum Nanoparticles. *J. Phys. Chem. Lett.* **2011**, *2*, 1460–1463.
- (25) Bertoncello, P.; Kefalas, E.; Pikramenou, Z.; Unwin, P.; Forster, R. Adsorption Dynamics and Electrochemical and Photophysical Properties of Thiolated Ruthenium 2,2'-Bipyridine Monolayers. *J. Phys. Chem. B* **2006**, *110*, 10063–10069.
- (26) Lo, K. K.-W.; Choi, A. W.-T.; Law, W. H.-T. Applications of Luminescent Inorganic and Organometallic Transition Metal Complexes as Biomolecular and Cellular Probes. *Dalton Trans.* **2012**, *41*, 6021–6047.
- (27) Filby, M. H.; Muldoon, J.; Dabb, S.; Fletcher, N. C.; Ashcroft, A. E.; Wilson, A. J. Protein Surface Recognition Using Geometrically Pure Ru(II) Tris(bipyridine) Derivatives. *Chem. Commun.* **2011**, *47*, 559–561.
- (28) Anfossi, L.; Baggiani, C.; Giovannoli, C.; Giraudi, G. Homogeneous Immunoassay Based on Gold Nanoparticles and Visible Absorption Detection. *Anal. Bioanal. Chem.* **2009**, *394*, 507–512.
- (29) Mendes, P. M. Stimuli-Responsive Surfaces for Bio-Applications. *Chem. Soc. Rev.* **2008**, *37*, 2512–2529.
- (30) Jetty, R.; Bandera, Y. P.; Daniele, M. A.; Hanor, D.; Hung, H.-I.; Ramshesh, V.; Duperreault, M. F.; Nieminen, A.-L.; Lemasters, J. J.; Foulger, S. H. Protein Triggered Fluorescence Switching of near-Infrared Emitting Nanoparticles for Contrast-Enhanced Imaging. *J. Mater. Chem. B* **2013**, *1*, 4542–4554.
- (31) Wang, C.; Ouyang, J.; Ye, D.-K.; Xu, J.-J.; Chen, H.-Y.; Xia, X.-H. Rapid Protein Concentration, Efficient Fluorescence Labeling and Purification on a Micro/Nanofluidics Chip. *Lab Chip* **2012**, *12*, 2664–2671.
- (32) Chung, C. Y.-S.; Yam, V. W.-W. Induced Self-Assembly and Forster Resonance Energy Transfer Studies of Alkynylplatinum(II) Terpyridine Complex through Interaction with Water-Soluble Poly(Phenylene Ethynylene Sulfonate) and the Proof-of-Principle Demonstration of This Two-Component Ensemble for Selective Label-Free Detection of Human Serum Albumin. *J. Am. Chem. Soc.* **2011**, *133*, 18775–18784.
- (33) Shi, H. Q.; Tsai, W. B.; Garrison, M. D.; Ferrari, S.; Ratner, B. D. Template-Imprinted Nanostructured Surfaces for Protein Recognition. *Nature* **1999**, *398*, 593–597.
- (34) Kober, E. M.; Caspar, J. V.; Sullivan, P. B.; Meyer, T. J. Synthetic Routes to New Polypridyl Complexes of Osmium(II). *Inorg. Chem.* **1988**, *27*, 4587–4598.
- (35) Sprouse, S.; King, K. A.; Spellane, P. J.; Watts, R. J. Photophysical Effects of Metal-Carbon σ Bonds in Ortho-Metalated Complexes of Ir(III) and Rh(III). *J. Am. Chem. Soc.* **1984**, *106*, 6647–6653.
- (36) Hong, Y.-R.; Gorman, C. B. Synthetic Approaches to an Isostructural Series of Redox-Active, Metal Tris(bipyridine) Core Dendrimers. *J. Org. Chem.* **2003**, *68*, 9019–9025.
- (37) Sullivan, B. P.; Salmon, D. J.; Meyer, T. J. Mixed Phosphine 2,2'-Bipyridine Complexes of Ruthenium. *Inorg. Chem.* **1978**, *17*, 3334–3341.
- (38) Gaudiello, J. G.; Bradley, P. G.; Norton, K. A.; Woodruff, W. H.; Bard, A. J. Electrochemistry in Liquid Sulfur Dioxide. 5. Oxidation of Bipyridine and Phenanthroline Complexes of Osmium, Ruthenium and Iron. *Inorg. Chem.* **1984**, *23*, 3–10.
- (39) Slinker, J. D.; Gorodetsky, A. A.; Lowry, M. S.; Wang, J.; Parker, S.; Rohl, R.; Bernhard, S.; Malliaras, G. G. Efficient Yellow Electro-chemiluminescence from a Single Layer of a Cyclometalated Iridium Complex. *J. Am. Chem. Soc.* **2004**, *126*, 2763–2767.
- (40) Kumar, A.; Biebuyck, H. A.; Whitesides, G. M. Patterning Self-Assembled Monolayers: Applications in Materials Science. *Langmuir* **1994**, *10*, 1498–1511.
- (41) Nazeeruddin, M. K.; Zakeeruddin, S. M.; Kalyanasundaram, K. Enhanced Intensities of the Ligand-to-Metal Charge-Transfer Transitions in Ru(III) and Os(III) Complexes of Substituted Bipyridines. *J. Phys. Chem.* **1993**, *97*, 9607–9612.
- (42) Creutz, C.; Chou, M.; Netzel, T. L.; Okumura, M.; Sutin, N. Lifetimes, Spectra, and Quenching of the Excited-States of Polypyridine Complexes of Iron(II), Ruthenium(II), and Osmium (II). *J. Am. Chem. Soc.* **1980**, *102*, 1309–1319.
- (43) Kober, E. M.; Sullivan, B. P.; Dressick, W. J.; Caspar, J. V.; Meyer, T. J. Highly Luminescent Polypyridyl Complexes of Osmium(II). *J. Am. Chem. Soc.* **1980**, *102*, 7385–7387.
- (44) Hou, Y.; Xie, P.; Wu, K.; Wang, J.; Zhang, B.; Cao, Y. Synthetic Control of the Photophysical and Photoelectrochemical Properties of Ruthenium(II) Polypyridyl Complexes. *Sol. Energy Mater. Sol. Cells* **2001**, *70*, 131–139.
- (45) Juris, A.; Balzani, V.; Barigelli, F.; Campagna, S.; Belser, P.; von Zelewsky, A. Ru(II) Polypyridine Complexes - Photophysics, Photochemistry, Electrochemistry, and Chemi-Luminescence. *Coord. Chem. Rev.* **1988**, *84*, 85–277.
- (46) Neve, F.; Crispini, A.; Campagna, S.; Serroni, S. Synthesis, Structure, Photophysical Properties, and Redox Behavior of Cyclo-metatalated Complexes of Iridium(III) with Functionalized 2,2'-Bipyridines. *Inorg. Chem.* **1999**, *38*, 2250–2258.
- (47) Lowry, M. S.; Goldsmith, J. I.; Slinker, J. D.; Rohl, R.; Pascal, R. A.; Malliaras, G. G.; Bernhard, S. Single-Layer Electrochemiluminescent Devices and Photoinduced Hydrogen Production from an Ionic Iridium(III) Complex. *Chem. Mater.* **2005**, *17*, 5712–5719.
- (48) King, K. A.; Watts, R. J. Dual Emission from an Ortho-Metalated Ir(III) Complex. *J. Am. Chem. Soc.* **1987**, *109*, 1589–1590.
- (49) Colombo, M. G.; Güdel, H. U. Synthesis and High-Resolution Optical Spectroscopy of Bis(2-(2-Thienyl)Pyridinato-C⁸,N')(2,2'-Bipyridine)Iridium(III). *Inorg. Chem.* **1993**, *32*, 3081–3087.
- (50) Kober, E. M.; Caspar, J. V.; Lumpkin, R. S.; Meyer, T. J. Application of the Energy Gap Law to Excited-State Decay of Osmium(II)-Polypyridine Complexes: Calculation of Relative Non-radiative Decay Rates from Emission Spectral Profiles. *J. Phys. Chem.* **1986**, *90*, 3722–3734.
- (51) Lumpkin, R. S.; Kober, E. M.; Worl, L. A.; Murtaza, Z.; Meyer, T. J. Metal-to-Ligand Charge-Transfer (MLCT) Photochemistry - Experimental-Evidence for the Participation of a Higher Lying MLCT State in Polypyridyl Complexes of Ruthenium(II) and Osmium(II). *J. Phys. Chem.* **1990**, *94*, 239–243.
- (52) Faiz, J. A.; Williams, R. M.; Silva, M. J. J. P.; De Cola, L.; Pikramenou, Z. A Unidirectional Energy Transfer Cascade Process in a Ruthenium Junction Self-Assembled by α - and β -Cyclodextrins. *J. Am. Chem. Soc.* **2006**, *128*, 4520–4521.
- (53) Haider, J. M.; Williams, R. M.; De Cola, L.; Pikramenou, Z. Vectorial Control of Energy-Transfer Processes in Metallocyclodextrin Heterometallic Assemblies. *Angew. Chem., Int. Ed.* **2003**, *42*, 1830–1833.
- (54) Nakamaru, K. Synthesis, Luminescence Quantum Yields, and Lifetimes of Trischelated Ruthenium(I) Mixed-Ligand Complexes

Including 3,3'-Dimethyl-2,2'-Bipyridyl. *Bull. Chem. Soc. Jpn.* **1982**, *55*, 2697–2705.

(55) Willey, T. M.; Vance, A. L.; Bostedt, C.; van Buuren, T.; Meulenborg, R. W.; Terminello, L. J.; Fadley, C. S. Surface Structure and Chemical Switching of Thioctic Acid Adsorbed on Au(111) as Observed Using near-Edge X-Ray Absorption Fine Structure. *Langmuir* **2004**, *20*, 4939–4944.

(56) Altman, M.; Zenkina, O. V.; Ichiki, T.; Iron, M. A.; Evmenenko, G.; Dutta, P.; van der Boom, M. E. Positive Constructs: Charges Localized on Surface-Confining Organometallic Oligomers. *Chem. Mater.* **2009**, *21*, 4676–4684.

(57) Yeung, C. L.; Iqbal, P.; Allan, M.; Lashkar, M.; Preece, J. A.; Mendes, P. M. Tuning Specific Biomolecular Interactions Using Electro-Switchable Oligopeptide Surfaces. *Adv. Funct. Mater.* **2010**, *20*, 2657–2663.

(58) Stenberg, E.; Persson, B.; Roos, H.; Urbaniczky, C. Quantitative Determination of Surface Concentration of Protein with Surface Plasmon Resonance Using Radiolabeled Proteins. *J. Colloid Interface Sci.* **1990**, *143*, 513–526.

(59) Lahiri, J.; Isaacs, L.; Tien, J.; Whitesides, G. M. A Strategy for the Generation of Surfaces Presenting Ligands for Studies of Binding Based on an Active Ester as a Common Reactive Intermediate: A Surface Plasmon Resonance Study. *Anal. Chem.* **1999**, *71*, 777–790.

(60) Davis, T. M.; Wilson, W. D. Determination of the Refractive Index Increments of Small Molecules for Correction of Surface Plasmon Resonance Data. *Anal. Biochem.* **2000**, *284*, 348–353.

(61) Peterlinz, K. A.; Georgiadis, R. In Situ Kinetics of Self-Assembly by Surface Plasmon Resonance Spectroscopy. *Langmuir* **1996**, *12*, 4731–4740.

(62) Dong, Y.; Abaci, S.; Shannon, C.; Bozack, M. J. Self-Assembly and Electrochemical Desorption of Thioctic Acid Monolayers on Gold Surfaces. *Langmuir* **2003**, *19*, 8922–8926.

(63) Alcock, N. W.; Barker, P. R.; Haider, J. M.; Hannon, M. J.; Painting, C. L.; Pikramenou, Z.; Plummer, E. A.; Rissanen, K.; Saarenketo, P. Red and Blue Luminescent Metallo-Supramolecular Coordination Polymers Assembled through $\pi-\pi$ Interactions. *Dalton Trans.* **2000**, 1447–1461.

(64) D'Aléo, A.; Williams, R. M.; Chriqui, Y.; Iyer, V. M.; Belser, P.; Vergeer, F.; Ruiz, V.; Unwin, P. R.; De Cola, L. Electrochemical and Photophysical Properties of Ruthenium(II) Bipyridyl Complexes with Pendant Alkanethiol Chains in Solution and Anchored to Metal Surfaces. *Open Inorg. Chem. J.* **2007**, *1*, 26–36.

(65) De Wolf, F. A.; Brett, G. M. Ligand-Binding Proteins: Their Potential for Application in Systems for Controlled Delivery and Uptake of Ligands. *Pharmacol. Rev.* **2000**, *52*, 207–236.

(66) Spector, A. A. Fatty-Acid Binding to Plasma Albumin. *J. Lipid Res.* **1975**, *16*, 165–179.

(67) Lo, K. K.-W.; Lee, T. K.-M.; Lau, J. S.-Y.; Poon, W.-L.; Cheng, S.-H. Luminescent Biological Probes Derived from Ruthenium(II) Estradiol Polypyridine Complexes. *Inorg. Chem.* **2008**, *47*, 200–208.

(68) Rogozea, A.; Matei, I.; Turcu, I. M.; Ionita, G.; Sahini, V. E.; Salifoglou, A. EPR and Circular Dichroism Solution Studies on the Interactions of Bovine Serum Albumin with Ionic Surfactants and Beta-Cyclodextrin. *J. Phys. Chem. B* **2012**, *116*, 14245–14253.